A Vision-Based Formation Control Framework

Aveek K. Das, *Student Member, IEEE*, Rafael Fierro, *Member, IEEE*, Vijay Kumar, *Senior Member, IEEE*, James P. Ostrowski, *Member, IEEE*, John Spletzer, and Camillo J. Taylor, *Member, IEEE*

***Abstract*—We describe a framework for cooperative control of a group of nonholonomic mobile robots that allows us to build complex systems from simple controllers and estimators. The resultant modular approach is attractive because of the potential for reusability. Our approach to composition also guarantees stability and convergence in a wide range of tasks. There are two key features in our approach: 1) a paradigm for switching between simple decentralized controllers that allows for changes in formation; 2) the use of information from a single type of sensor, an omnidirectional camera, for all our controllers. We describe estimators that abstract the sensory information at different levels, enabling both decentralized and centralized cooperative control. Our results include numerical simulations and experiments using a testbed consisting of three nonholonomic robots.**

***Index Terms*—Cooperative localization, formation control, hybrid control, nonholonomic mobile robots.**

I. Introduction

THE LAST FEW years have seen active research in the field of control and coordination for multiple mobile robots, with applications including tasks such as exploration [1], surveillance [2], search and rescue [3], mapping of unknown or partially known environments, distributed manipulation [4], [5], and transportation of large objects [6], [7]. While robot control is considered to be a well-understood problem area [8], [9], most of the current success stories in multirobot coordination do not rely on or build on the results available in the control theory and dynamical systems literature. This is because traditional control theory primarily enables the design of controllers in a single mode of operation, in which the task and the model of the system are fixed [10]. When operating in unstructured or dynamic environments with many different sources of uncertainty, it is very difficult if not impossible to design controllers that will guarantee performance even in a local sense. In contrast, we know that one can readily design reactive controllers or behaviors that react to simple stimuli or commands from the environment. Successful applications of this idea are found in subsumption architectures [11], behavior-based robotics [12], and other works [13].

In this paper, we address the development of intelligent robot systems by composing simple building blocks in a *bottom-up approach*. The building blocks consist of controllers and estimators, and the framework for composition allows for tightly coupled perception-action loops. While this philosophy is similar in spirit to a behavior-based control paradigm [12], we differ in the more formal, control-theoretic approach in developing the basic components and their composition.

The goal of this paper is to develop a framework for composition of simple controllers and estimators to control the formation of a group of robots. By formation control, we simply mean the problem of controlling the relative positions and orientations of robots in a group, while allowing the group to move as a whole. Problems in formation control that have been investigated include assignment of feasible formations [14], [15], moving into formation [16], maintenance of formation shape [17], [18], and switching between formations [19], [20]. Approaches to modeling and solving these problems have been diverse, ranging from paradigms based on combining reactive behaviors [12], [21] to those based on leader-follower graphs [17], [19] and virtual structures [22], [23].

We are particularly interested in applications like *cooperative manipulation*, where a semirigid formation may be necessary to transport a grasped object to a prescribed location, and *cooperative mapping*, where the formation may be defined by a set of sensor constraints. We consider situations in which there is no global positioning system and the main sensing modality is vision. Our platform of interest is a car-like robot with a single physical sensor, an omnidirectional camera.

Our contributions in this paper are two-fold. First, we develop a control-theoretic *bottom-up approach* to building and composing controllers and estimators. These include simple decentralized, reactive controllers for obstacle avoidance, collision recovery, and pursuing targets, and more complex controllers for maintaining formation. These controllers can be either centralized or decentralized and are derived from input–output linearization [10]. Our second contribution is a *framework for multirobot coordination* that allows robots to maintain or change formation while following a specified trajectory and to perform cooperative manipulation tasks. Our framework involves a sequential composition of controllers, or modes, and we show that the dynamics of the resulting switched system are stable and converge to the desired formation.

The paper is organized as follows. In Section II, we state the assumptions of our control framework and present details on our

Manuscript received March 22, 2002. This paper was recommended for publication by Associate Editor T. Arai and Editor S. Hutchinson upon evaluation of the reviewers' comments. This work was supported by the Defense Advanced Research Projects Agency ITO MARS Program under Grant 130-1303-4-534328-xxxx-2000-0000, the Air Force Office of Scientific Research under Grant F49620-01-1-0382, and the National Science Foundation under Grant CDS-97-03220 and Grant IIS 987301. This paper was presented in part at the IEEE International Conference on Robotics and Automation, Seoul, Korea, May, 2001.

A. K. Das, V. Kumar, J. P. Ostrowski, J. Spletzer, and C. J. Taylor are with the GRASP Laboratory, University of Pennsylvania, Philadelphia, PA 19104-6228 USA (e-mail: aveek@grasp.cis.upenn.edu; kumar@grasp.cis.upenn.edu; jpo@grasp.cis.upenn.edu; spletzer@grasp.cis.upenn.edu; cjtaylor@grasp.cis.upenn.edu).

R. Fierro is with the MARHES Laboratory, School of Electrical and Computer Engineering, Oklahoma State University, Stillwater, OK 74078-5032 USA (e-mail: rfierro@okstate.edu).

Digital Object Identifier 10.1109/TRA.2002.803463

controllers for formation control. We discuss the assignment of formations, changes in formations, and stable switching strategies in Section III using a group of three robots as an example. Section IV addresses our sensing and estimation schemes for formation control. Hardware details and experimental results illustrating the application of our multirobot coordination framework are in Section V. Finally, in Section VI, we draw conclusions and suggest future work.

II. Control Algorithms

Before describing the individual components of our control framework, we list several important assumptions concerning the group of robots and the formation. We assume, as in [17], the robots are labeled and one of the robots, designated as R_1, is the lead (or reference) robot. The lead robot's motion defines the bulk motion of the group. The motion of individual members within the formation is then described in reference to the lead robot. As in [17] and [19], the relationship between a robot and its neighboring robots is described by a *control graph*. The control graph is an acyclic, directed graph with robots as nodes, R_1 as the parent node, and edges directed from nodes with smaller integer label values to those with with larger integer values. Each edge denotes a constraint between the robots connected by the edge and a controller that tries to maintain the constraint. We present more details on control graphs in the following sections.

In this section, we describe control algorithms that specify the interactions between each robot and its neighbor(s) or the environment. The robots are velocity-controlled nonholonomic car-like platforms and have two independent inputs. The control laws are motivated by ideas from the well-established area of input–output feedback linearization [10]. This means we can regulate two outputs. The kinematics of the ith robot can be abstracted as a unicycle model (other models can be adapted to this framework)

$$\dot{x}_i = v_i \cos\theta_i, \quad \dot{y}_i = v_i \sin\theta_i, \quad \dot{\theta}_i = \omega_i \tag{1}$$

where we let $\boldsymbol{x}_i = (x_i,\ y_i,\ \theta_i) \in SE(2)$, and v_i and ω_i are the linear and angular velocities, respectively.

A. Basic Leader-Following Control

We start with a simple leader-follower configuration (see Fig. 1) (denoted $SB_{ij}C$), in which robot R_j follows R_i with a desired *S*eparation l_{ij}^d and desired relative *B*earing ψ_{ij}^d. Note that this relative bearing describes the heading direction of the follower with respect to the leader. The two-robot system is transformed into a new set of coordinates where the state of the leader is treated as an exogenous input. Thus, the kinematic equations are given by

$$\dot{\boldsymbol{z}}_{ij} = \boldsymbol{G}_1(\boldsymbol{z}_{ij}, \beta_{ij})\,\boldsymbol{u}_j + \boldsymbol{F}_1(\boldsymbol{z}_{ij})\,\boldsymbol{u}_i, \qquad \dot{\beta}_{ij} = \omega_i - \omega_j \tag{2}$$

where $\boldsymbol{z}_{ij} = [\,l_{ij} \quad \psi_{ij}\,]^T$ is the system output, $\beta_{ij} = \theta_i - \theta_j$ is the relative orientation, $\boldsymbol{u}_j = [\,v_j \quad \omega_j\,]^T$ is the input for R_j, $\boldsymbol{u}_i = [\,v_i \quad \omega_i\,]^T$ is R_i's input, and

$$\boldsymbol{G}_1 = \begin{pmatrix} \cos\gamma_{ij} & d\sin\gamma_{ij} \\ \frac{-\sin\gamma_{ij}}{l_{ij}} & \frac{d\cos\gamma_{ij}}{l_{ij}} \end{pmatrix}, \qquad \boldsymbol{F}_1 = \begin{pmatrix} -\cos\psi_{ij} & 0 \\ \frac{\sin\psi_{ij}}{l_{ij}} & -1 \end{pmatrix}$$

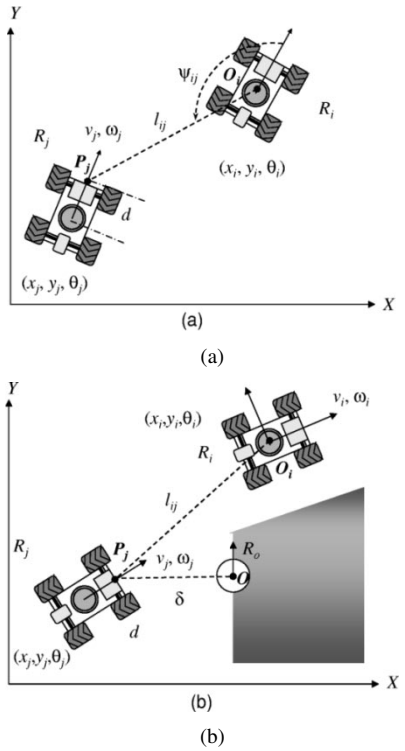

Fig. 1. Two robots using (a) basic leader-following controller and (b) the leader-obstacle controller.

with $\gamma_{ij} = \beta_{ij} + \psi_{ij}$. By applying input–output feedback linearization, the control velocities for the *follower* are given by

$$\boldsymbol{u}_j = \boldsymbol{G}_1^{-1}(\boldsymbol{p}_1 - \boldsymbol{F}_1\boldsymbol{u}_i) \tag{3}$$

where d is the offset to an off-axis *reference* point P_j on the robot and $\boldsymbol{p}_1$ is an auxiliary control input given by

$$\boldsymbol{p}_1 = \begin{pmatrix} k_1\left(l_{ij}^d - l_{ij}\right) \\ k_2\left(\psi_{ij}^d - \psi_{ij}\right) \end{pmatrix} = \boldsymbol{k}\left(\boldsymbol{z}_{ij}^d - \boldsymbol{z}_{ij}\right).$$

k_1 and $k_2 > 0$ are the user-selected controller gains. The closed-loop linearized system is simply given by

$$\dot{\boldsymbol{z}}_{ij} = \boldsymbol{p}_1 = \boldsymbol{k}\left(\boldsymbol{z}_{ij}^d - \boldsymbol{z}_{ij}\right), \qquad \dot{\beta}_{ij} = \omega_i - \omega_j. \tag{4}$$

In the following, we prove that under suitable assumptions on the motion of the lead robot, the closed-loop system is stable. Since we are using input–output feedback linearization [10], the output vector $\boldsymbol{z}_{ij}$ will converge to the desired value $\boldsymbol{z}_{ij}^d$ arbitrarily fast. However, a complete stability analysis requires the study of the internal dynamics of the robot, i.e., the relative orientation β_{ij}.

Theorem 1: Assume that the lead vehicle's linear velocity along the path $g(t) \in SE(2)$ is lower bounded, i.e., $v_i > 0$, its angular velocity is bounded, i.e., $\|\omega_i\| < W_{\max}$, and the initial relative heading is bounded away from $\pm\pi$, i.e., $|\beta_{ij}(0)| < c_1\pi$, for some $c_1 < 1$. If the control input (3) is applied to R_j, then the system described by (2) is stable and the output $\boldsymbol{z}_{ij}$ in (4) converges exponentially to the desired value $\boldsymbol{z}_{ij}^d$.

Proof: Let the system error $\boldsymbol{e} = [\,e_1 \quad e_2 \quad e_3\,]^T$ be defined as

$$e_1 = l_{ij}^d - l_{ij}, \quad e_2 = \psi_{ij}^d - \psi_{ij}, \quad e_3 = \beta_{ij}. \tag{5}$$

By looking at (4), we have that e_1 and e_2 converge to zero exponentially. Then, we need to show that the internal dynamics

of R_j are stable, which is equivalent to showing that the orientation error e_3 is bounded. Thus, we have

$$\dot{e}_3 = \omega_i - \omega_j$$

and, after some algebraic simplification, we obtain

$$\dot{e}_3 = -\frac{v_i}{d}\sin e_3 + \eta_1(\omega_i, e_1, e_2, e_3) \tag{6}$$

where

$$\eta_1 = \omega_i\left(1 - \frac{l_{ij}}{d}\cos(e_3 + \psi_{ij})\right) - \frac{1}{d}\left(k_1 e_1 \sin(e_3 + \psi_{ij}) + k_2 e_2 l_{ij}\cos(e_3 + \psi_{ij})\right).$$

The nominal system, i.e., $\eta_1(t, e_3) = 0$ is given by

$$\dot{e}_3 = -\frac{v_i}{d}\sin e_3 \tag{7}$$

which is (locally) exponentially stable if the velocity of the lead robot $v_i > 0$ and $\|e_3\| < \pi$. Since ω_i is bounded, one can show that $\|\eta_1(t, e_3)\| \le \delta_1$. Using stability theory of perturbed systems [10] and the condition $|\beta_{ij}(0)| < c_1\pi$, gives [20]

$$\|e_3(t)\| \le \sigma_1, \quad \forall t \ge t_1$$

for some finite time t_1 and positive number σ_1. ■

Remark 1: The above theorem shows that, under some reasonable assumptions, the two-robot system is stable, i.e., there exists a Lyapunov function $V(t, \boldsymbol{e}) \in [0, \infty) \times D$, where $D = \{\boldsymbol{e} \in \mathbb{R}^3 | \|\boldsymbol{e}\| < c\}$ and $c > 0$, such that $\dot{V}(t, \boldsymbol{e}) \le 0$.

We can study some particular formations of practical interest. For example, if the leader travels in a straight line, i.e., $\omega_i = 0$, it can be shown that the system is (locally) asymptotically stable, i.e., $e_3 \to 0$ as $t \to \infty$, provided that $v_i > 0$ and $\|e_3\| < \pi$. If ω_i is constant (*circular motion*), then e_3 is bounded. It is well known that an optimal nonholonomic path can be planned by joining linear and circular trajectory segments. Hence, any trajectory generated by such a planner for the leader will ensure stable leader-follower dynamics using the above controller.

Remark 2: This result can be extended to n robots in an inline, convoy-like formation where R_i follows R_{i-1} under $SB_{i-1,i}C$. If each successive leader's trajectory satisfies the assumptions of *Theorem 1*, then the convoy-like system can be shown to be stable. We will provide some more insight into stabilizing n robot formations at the end of this section.

B. Leader-Obstacle Control

This controller (denoted SD_oC) allows the follower to avoid obstacles while following a leader with a desired separation. Thus, the outputs of interest are the separation l_{ij} and the distance δ between the reference point P_j on the follower, and the closest point O on the object. We define a *virtual* robot R_o as shown in Fig. 1 (right), which moves on the obstacle's boundary. We define θ_o as the heading of the virtual robot, which is defined locally by the tangent to the obstacle's boundary. Our previous estimation strategies for wall following [24] can be adapted to recover the relative orientation to the closest sensed section of the object's boundary. For this case, the kinematic equations are given by

$$\dot{\boldsymbol{z}}_{ij} = \begin{pmatrix} \cos\gamma_{ij} & d\sin\gamma_{ij} \\ \sin\gamma_{oj} & d\cos\gamma_{oj} \end{pmatrix}\boldsymbol{u}_j + \begin{pmatrix} -v_i\cos\psi_{ij} \\ 0 \end{pmatrix}, \quad \dot{\theta}_j = \omega_j \tag{8}$$

where $\boldsymbol{z}_{ij} = [\, l_{ij} \quad \delta \,]^T$ is the system output, $\boldsymbol{u}_j = [\, v_j \quad \omega_j \,]^T$ is the input for R_j, and $\gamma_{oj} = \theta_o - \theta_j$, $\gamma_{ij} = \beta_{ij} + \psi_{ij}$. By applying input–output feedback linearization as above, but replacing the auxiliary control input, $\boldsymbol{p}_1$, with $\boldsymbol{p}_2$, given by

$$\boldsymbol{p}_2 = \begin{pmatrix} k_1\left(l_{ij}^d - l_{ij}\right) \\ k_o\left(\delta^d - \delta\right) \end{pmatrix} = \boldsymbol{k}\left(\boldsymbol{z}_{ij}^d - \boldsymbol{z}_{ij}\right)$$

(k_1, $k_o > 0$ are controller gains), the closed-loop linearized system is given by

$$\dot{\boldsymbol{z}}_{ij} = \boldsymbol{p}_2 = \boldsymbol{k}\left(\boldsymbol{z}_{ij}^d - \boldsymbol{z}_{ij}\right), \qquad \dot{\theta}_j = \omega_j. \tag{9}$$

Remark 3: It is worth noting that feedback input–output linearization is possible as long as $d\cos(\gamma_{oj} - \gamma_{ij}) \ne 0$, i.e., the controller is not defined if $\gamma_{oj} - \gamma_{ij} = \pm k\pi/2$. This occurs when vectors $O\vec{P}_j$ and $O_i\vec{P}_j$ are collinear, which should never happen in practice.

Remark 4: By using this controller, a follower robot will avoid the nearest obstacle within its field of view while keeping a desired distance from the leader. This is a reasonable assumption for many outdoor environments of practical interest. While there are obvious limitations to this scheme in maze-like environments, it is not difficult to characterize the set of obstacles and leader trajectories for which this scheme will work.

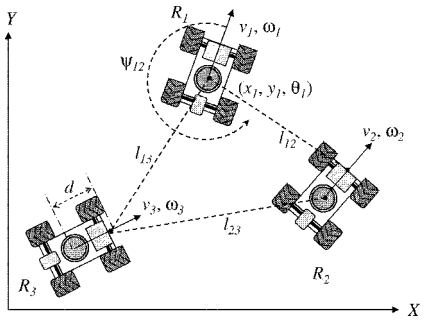

Fig. 2. Three-robot formation controller.

C. Three-Robot Shape Control

Consider a formation of three nonholonomic robots labeled R_1, R_2, and R_3 (see Fig. 2). There are several possible approaches to controlling the formation. For example, one could use two basic lead-follower controllers: either $SB_{12}C$ with $SB_{13}C$, or $SB_{12}C$ with $SB_{23}C$. Another approach that is more robust to noise is to use a three-robot formation shape controller (denoted $S_{13}S_{23}C$), that has robot R_3 follow both R_1 and R_2 with desired separations l_{13}^d and l_{23}^d, respectively, while R_2 follows R_1 with $SB_{12}C$. Again, the kinematic equations are given by

$$\begin{aligned} \dot{\boldsymbol{z}} &= \boldsymbol{G}_2(\boldsymbol{z}, \theta_1, \theta_2, \theta_3)\boldsymbol{u}_{23} + \boldsymbol{F}_2(\boldsymbol{z})\boldsymbol{u}_1, \\ \dot{\theta}_2 &= \omega_2, \quad \dot{\theta}_3 = \omega_3 \end{aligned} \tag{10}$$

where $\boldsymbol{z} = [\, l_{12} \quad \psi_{12} \quad l_{13} \quad l_{23} \,]^T$ is the system output, $\boldsymbol{u}_{23} = [\, v_2 \quad \omega_2 \quad v_3 \quad \omega_3 \,]^T$ is the input vector, and

$$\boldsymbol{G}_2 = \begin{pmatrix} \cos\gamma_{12} & d\sin\gamma_{12} & 0 & 0 \\ \frac{-\sin\gamma_{12}}{l_{12}} & \frac{d\cos\gamma_{12}}{l_{12}} & 0 & 0 \\ 0 & 0 & \cos\gamma_{13} & d\sin\gamma_{13} \\ -\cos\psi_{23} & 0 & \cos\gamma_{23} & d\sin\gamma_{23} \end{pmatrix}$$

$$\boldsymbol{F}_2 = \begin{pmatrix} -\cos\psi_{12} & 0 \\ \frac{\sin\psi_{12}}{l_{12}} & -1 \\ -\cos\psi_{13} & 0 \\ 0 & 0 \end{pmatrix}$$

Once again we use input–output linearization to derive a control law for $\boldsymbol{u}_{23}$ which gives us the following closed-loop dynamics:

$$\dot{\boldsymbol{z}} = \boldsymbol{p}_3, \quad \dot{\theta}_2 = \omega_2, \quad \dot{\theta}_3 = \omega_3 \tag{11}$$

where $\boldsymbol{p}_3 = \boldsymbol{k}(\boldsymbol{z}^d - \boldsymbol{z})$ is an auxiliary control input and $\boldsymbol{k}$ is the chosen positive definite controller gain matrix. As before, we will show that the closed-loop system is stable and the robots navigate keeping formation.

Theorem 2: Assume that the lead vehicle's linear velocity along the path $g(t) \in SE(2)$ is lower bounded, i.e., $v_1 > 0$, its angular velocity is also bounded, i.e., $||\omega_1|| < W_{\max}$, and the initial relative orientation $|\theta_1(0) - \theta_j(0)| < c_j\pi$ with $c_j < 1$ and $j = 2, 3$. If the control input $\boldsymbol{u}_{23}$ obtained from the feedback linearization is applied to R_2 and R_3, then the formation is stable and the system output $\boldsymbol{z}$ in (11) converges exponentially to the desired value $\boldsymbol{z}^d$.

Proof: By *Theorem 1*, the internal dynamics of R_2 are stable, i.e., the orientation error $(\theta_1 - \theta_2)$ is bounded. As a result for R_3, the relative velocities and orientations of R_1 and R_2 can be shown to be bounded under the assumptions of the theorem. By an analysis similar to *Theorem 1*, the internal dynamics of R_3 can be shown to be stable (see [20] for details).

Remark 5: In contrast to the previous two-robot formation controller, this controller allows explicit control of all separations and minimizes the risk for collisions. Hence, it is preferred when the separations between robots are small, and when, coincidentally, the estimates of distance through vision are better.

Remark 6: *Theorems 1* and *2* guarantee that all signals in the closed-loop formation system are bounded and the output error vanishes exponentially. However, as in any practical system, unmodeled dynamics and measurement errors will degrade performance. The best we can do is guarantee that the output error converges to a neighborhood of the origin. Robust control theory applied to nonholonomic systems (e.g., [25]) points to a systematic way of approaching this problem analytically. As can be seen from our experimental results, since velocities of individual robots and sensor errors are bounded, the system errors are also bounded.

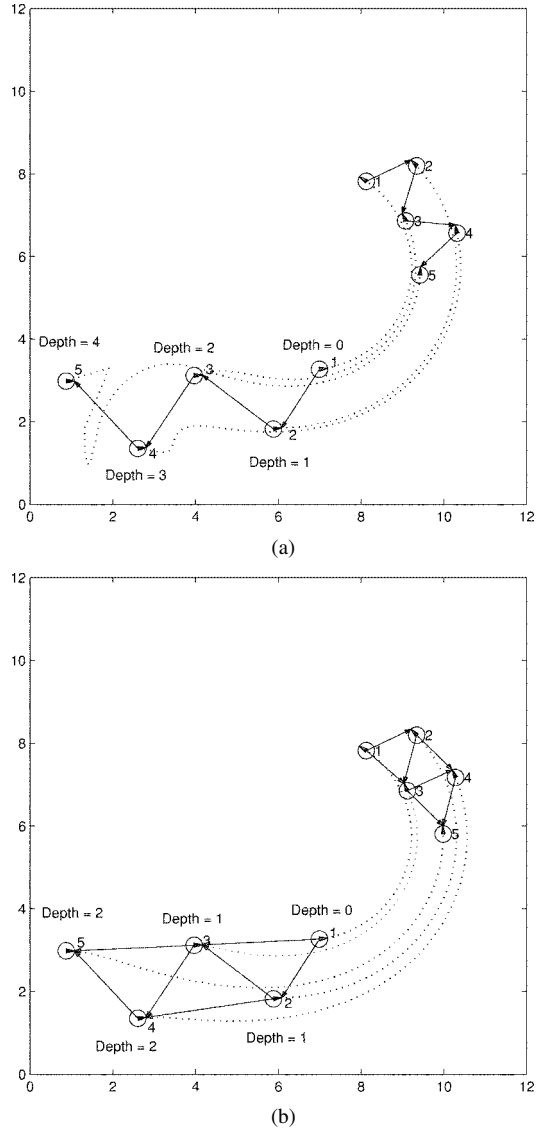

Fig. 3. Five-robot formation. (a) All *SBC* controller chains. (b) One *SBC* and four *SSC* controllers. For the same leader trajectory, notice the higher transient formation shape errors for the control graph (a).

D. Extension to n Robots

Results similar to *Theorems 1* and *2* are possible for formations of $n > 3$ robots, but they have to be hand crafted, i.e., there currently are no general results. Instead, we present a discussion on propagation of stability bounds and formation shape errors along the leader-follower chains in a given formation.

As we saw earlier in this section, to guarantee stability of the internal dynamics of a robot R_{k+1} following R_k using *SBC*, we need $v_k > 0$ and $|\omega_k| < W_{k,\max}$. This, in turn, means that v_{k-1} and ω_{k-1} will have to be appropriately constrained, e.g., $v_{k-1} > V_{k-1,\min}$ and $|\omega_{k-1}| < W_{k-1,\max}$. Notice it is not enough that $v_{k-1} > 0$, but instead $v_{k-1} > V_{k-1,\min}$ where $V_{k-1,\min}$ will depend on the initial formation error, controller gains, and $W_{k-1,\max}$. This idea can be applied to an n robot inline formation. Basically, the smaller the initial formation errors and the smoother the leader's trajectory, the easier it is to maintain a formation shape.

Thus, the performance associated with a choice of formation for nonholonomic robots with input–output feedback linearized controllers depends on the length of the path for flow of control information (feedforward terms) from the leader to any follower in the assigned formation. As this length becomes greater, the formation shape errors have a tendency to grow. This leads to a simple heuristic: when deciding between two formation control assignments that are otherwise similar, we prefer the one that minimizes the length of leader-follower chains (we prefer $S_{ik}S_{jk}C$ over $SB_{ik}C$ or $SB_{jk}C$ whenever possible, see Fig. 3 for an example). We revisit the n robot formation assignment problem in the next section using the notion of control graphs. We consider two types of scenarios: the control graph is fixed, and where the control graph is dynamically adapted to the environment and the relative robot positions.

III. Coordination Protocol

In Section II, we have shown that under certain assumptions a group of robots can navigate maintaining a stable formation. However, in real situations mobile robotic systems are subject

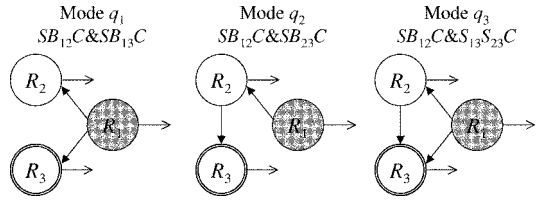

Fig. 4. Three control graphs for the three-robot case.

to dynamic sensor, actuator, and communication constraints. We need a switching paradigm that allows robots to select the most appropriate controllers (formation) depending on the environment. We first illustrate this approach using three nonholonomic mobile robots R_1, R_2, and R_3.

A. Choice of Formations: A Switching Strategy

Let $U_j = \{\xi_{1,j}, \ldots, \xi_{p,j}\}$ be the set of available controllers for robot R_j. We consider the problem of selecting the controller, $\xi_{k,j} \in U_j$ for robot R_j, assuming that the controllers for robots $R_2, R_3, \ldots, R_{j-1}$ have been specified.

First, R_1, the reference robot, follows a given trajectory $g(t) \in SE(2)$. Since R_2 can only follow R_1 (because of the numbering constraint of Section II), $U_2 = \{SB_{12}C\}$. Thus, R_2 follows R_1 with $SB_{12}C$. The set for R_3 now has three controllers: $U_3 = \{SB_{13}C, SB_{23}C, S_{13}S_{23}C\}$. Thus, as shown in Fig. 4, R_3 may follow R_1 or R_2 with $SB_{13}C$ or $SB_{23}C$, or follow both R_1 *and* R_2 with $S_{13}S_{23}C$. The palette of controllers for the three-robot group becomes $U = \{U_2 \times U_3\}$. Each member of this palette corresponds to a different control graph and a different mode.

If the assumptions in *Theorems 1* and *2* hold, then each mode q_i with $i = 1, 2, 3$ is stable. We need to show that for a given switching strategy S_w, the switched system is stable, i.e., given any initial mode q_i^0, a desired mode q_i^d is achieved in finite time.

Our switching strategy is guided primarily by our sensor (omnidirectional camera) constraints and the presence of obstacles. Fig. 5 depicts the switching boundaries in Cartesian space where r_2 denotes the maximum range within which a neighbor robot can be detected. $r_1 < r_2$ is a predefined range where a robot may detect two possible leaders. To be more specific, R_3 may detect R_1, R_2, neither robot, or both. Notice also that the triangle inequality $l_{ik} + l_{jk} > l_{ij}$ should be satisfied. If R_i with $i = 1, 2, 3$ were collinear, *SSC* would not be defined, then a *SBC* should be utilized.

The formation control objective is to drive R_3 to a region Ω_3 where it can detect both R_1 and R_2, i.e., mode q_3. Thus, the switching control strategy for R_3 can be summarized as follows:

$$\begin{aligned}
&\textbf{If } (l_{13} < l_{23}) \& (l_{23} > r_1) \& (l_{13} < r_2), \textbf{ Then } SB_{13}C \\
&\textbf{If } (l_{13} > l_{23}) \& (l_{13} > r_1) \& (l_{23} < r_2), \textbf{ Then } SB_{23}C \\
&\textbf{If } (l_{13} < r_1) \& (l_{23} < r_1), \textbf{ Then } S_{13}S_{23}C \\
&\textbf{If } (l_{13} > r_2) \& (l_{23} > r_2), \textbf{ Then } \text{Autonomous Navigation}.
\end{aligned} \tag{12}$$

The set of control behaviors that a robot uses when there is no leader within its field of view is called autonomous navigation.

Since a palette of controllers and a switching strategy are given, we need to verify that the switched system will reach mode q_3, regardless of the initial mode. Let $\boldsymbol{x}_0 \in \Omega_3$ be the desired position of R_3. The key idea is that the three modes in Fig. 4 share the same *goal* position $\boldsymbol{x}_0$. Thus, R_3 is always driven to the region where it can see and follow both R_2 and R_3. This intuitive procedure may fail if the switching strategy S_w is not properly defined. It is well known that a switched system can be unstable even though all individual systems are stable (see [26] and the references therein). For this particular switched system, we have the following result.

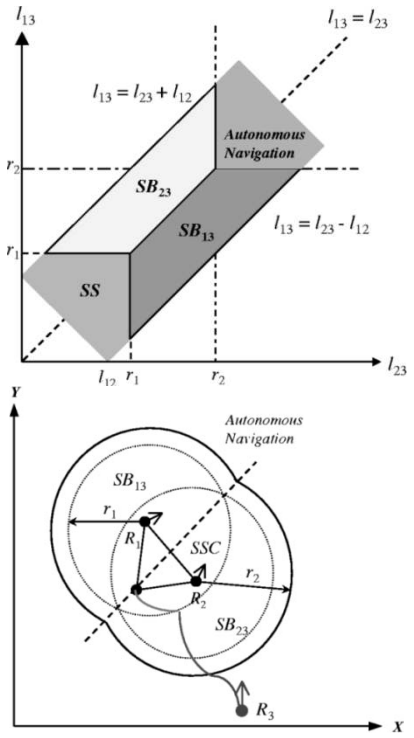

Fig. 5. Choice of controllers for R_3. The plot on the bottom shows the constraints and equilibrium point in Cartesian $x - y$ coordinates.

Proposition 3: Given the three-robot system depicted in Fig. 4, if the switching strategy (12) is applied to R_3 and all modes share the same goal position $\boldsymbol{x}_0 \in \Omega_3$, then for any initial mode $q_i(0)$, the switched system will reach q_3 in finite time, i.e., q_3 is a *stable* equilibrium mode.

Proof: Let the system error be defined as

$$\begin{aligned}
e_1 &= l_{13}^d - l_{13} \quad e_2 = \psi_{13}^d - \psi_{13}, \quad e_3 = \theta_1 - \theta_3 \\
e_4 &= l_{23}^d - l_{23}, \quad e_5 = \psi_{23}^d - \psi_{23}, \quad e_6 = \theta_2 - \theta_3 \\
e_7 &= l_{12}^d - l_{12}, \quad e_8 = \psi_{12}^d - \psi_{12}, \quad e_9 = \theta_1 - \theta_2
\end{aligned}$$

and a Lyapunov function candidate for the desired formation $\mathcal{F}_3$ be given by

$$V(\boldsymbol{e}) = V_3 + V_{12} \tag{13}$$

where

$$V_3 = \frac{1}{2}\left[e_1^2 + e_4^2 + e_3^2\right], \quad V_{12} = \frac{1}{2}\left[e_7^2 + e_8^2 + e_9^2\right]. \tag{14}$$

V_{12} is a Lyapunov function candidate for subsystem $SB_{12}C$, i.e., R_2 follows R_1 using a basic leader-following controller. If the assumptions in *Theorem 1* are satisfied, then $\dot{V}_{12} \leq 0$. Moreover, if the assumptions in *Theorem 2* are satisfied for subsystem $S_{13}S_{23}C$, then $\dot{V}_3 \leq 0$. Since $SB_{12}C$ is common for all modes, we only need to consider V_3 in (14) for studying the stability of the switched system.

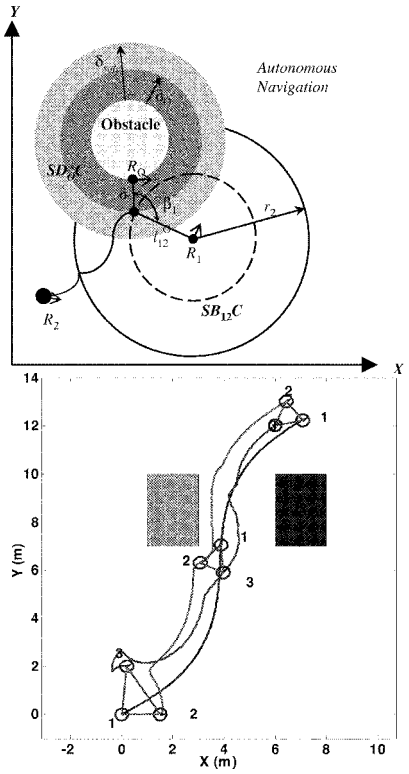

Fig. 6. Choice of controllers for R_2 in the presence of obstacles (top). In simulation, the leader follows a sinusoidal trajectory while followers switch to avoid obstacle and maintain the desired triangular formation (bottom).

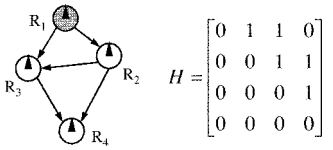

Fig. 7. Formation control graph for four robots and associated adjacency matrix.

By definition V_3 is a Lyapunov function for mode q_3. We would like to show that V_3 is also a Lyapunov function for q_1 and q_2. Let us consider formation mode q_1. $SB_{13}C$ makes $e_1 \to 0$ and $e_2 \to 0$ exponentially as $t \to \infty$. But we need to show that $e_4 \to 0$. To accomplish this, let us define $V_4 = 1/2(e_4^2)$, then show that $\dot{V}_4 = e_4\dot{e}_4 \leq 0$ or $(l_{23}^d - l_{23})\dot{l}_{23} \geq 0$. Since all modes share the same goal position $\boldsymbol{x}_0$, we have that ψ_{13}^d is given by

$$\psi_{13}^d = \cos^{-1}\left(\frac{l_{12}^{d\,2} + l_{13}^{d\,2} - l_{23}^{d\,2}}{2l_{12}^d l_{13}^d}\right) + \psi_{12}^d. \qquad (15)$$

Thus, $l_{23} \to l_{23}^d$ as $e_2 \to 0$. Using the inequality constraint imposed by the geometry of the problem, i.e., $l_{23}^d < l_{12}^d + l_{13}^d$, it is easy to show that $\dot{V}_4 = e_4\dot{e}_4 \leq 0$. Then, V_3 is a Lyapunov function for q_1 (similarly for q_2). More precisely, (13) is a common Lyapunov function for the switched system, and q_3 is stable for any arbitrary fast switching sequence. ■

Remark 7: It is well known that Lyapunov methods provide conservative stability regions, since we always consider the worst case. Simulation results reveal that the desired formation is achieved even when some of the assumptions discussed here are not satisfied, e.g., position and orientation of R_2 and R_3 are randomly initialized.

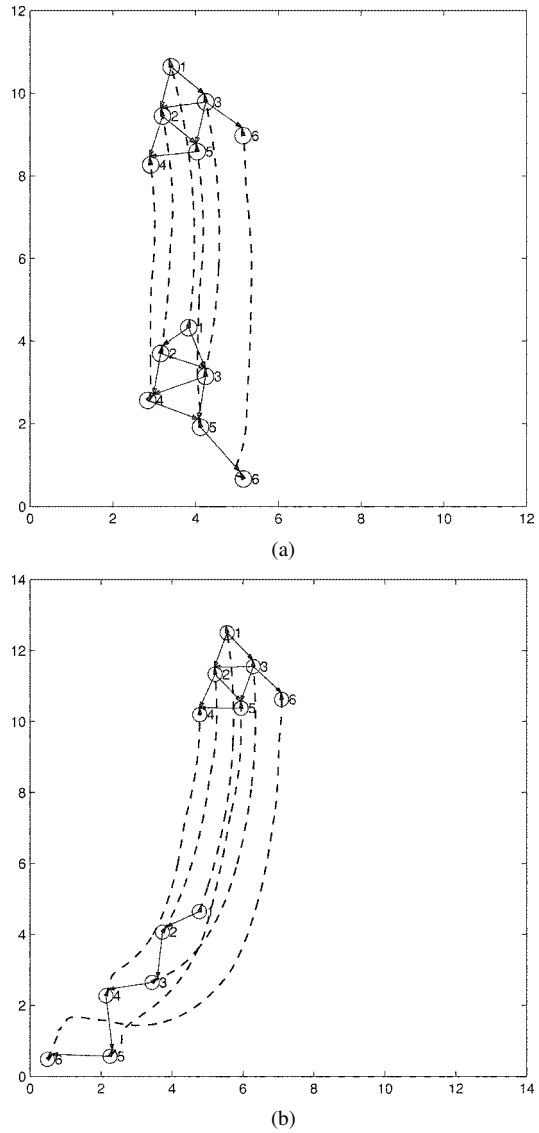

Fig. 8. (a) Six robots have an initial configuration close to the desired formation shape (an equilateral triangle with equally spaced robots). (b) The initial configuration is quite different from the desired formation shape.

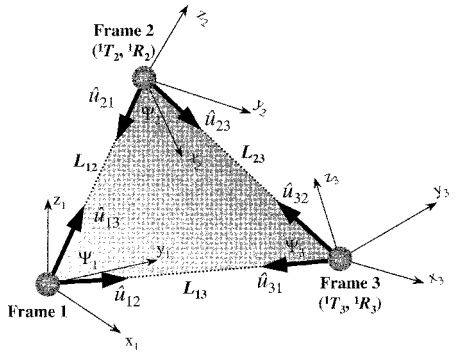

Fig. 9. Three-dimensional geometry for agent localization.

Fig. 6 depicts the switching boundaries in the presence of obstacles. Here, δ_{safe} denotes a safety region within which an obstacle can be detected, δ_o is the desired distance from the robot to the obstacle, and β_{1o} is the angle between $\vec{\delta}$ and $\vec{l_{12}}$. Let us assume R_2 follows R_1 with $SB_{12}C$, if an obstacle is detected,

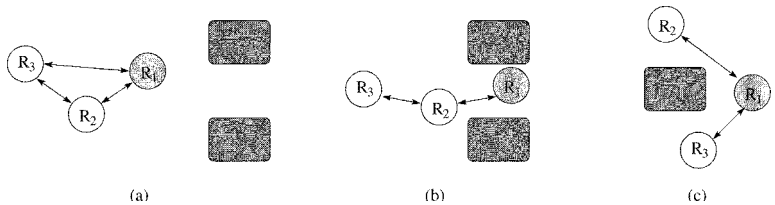

Fig. 10. Triangular to pair-wise localization switch resulting from team geometry (a)–(b) or occlusions in the environment (c).

then R_2 switches to SD_OC. Once the obstacle has been successfully negotiated, R_2 switches back to $SB_{12}C$ according to the following switching rules:

If $(\delta < \delta_{\text{safe}}) \& (\beta_{1o} < \pi) \& (l_{12} < r_2)$, **Then** SD_OC

If $(l_{12} > r_2) \& (\delta < \delta_{\text{safe}})$, **Then** $SB_{12}C$

If $(l_{12} > r_2) \& (\delta > \delta_{\text{safe}})$, **Then** Autonomous Navigation.

We now illustrate the application of these concepts to a simulation of three nonholonomic robots with one obstacle [Fig. 6 (bottom)]. Robot R_1 is the lead robot and the desired shape is an equilateral triangle. The formation shape is achieved and the robots successfully negotiate the obstacle. During the course of the motion, robot R_2 switches modes to successfully navigate the obstacle, while robot R_3 switches modes based on its location with respect to the lead robot, R_1.

B. Formation Control Graphs

When $n > 3$, we can construct more complex formations by using the same set of controllers and similar switching strategies. However, we need a representation of an n robot formation which scales easily with n and allows decentralized decision making. At the coordination level, for an n robot formation to maintain a desired shape, we need to model the choice of controllers between the individual robots as they move in a given environment. We use directed graphs to accomplish this [17].

We model the group of n autonomous mobile robots as a tuple $\mathcal{F} = (g, \boldsymbol{r}, H)$ where $g(t) \in SE(2)$ (or, e.g., $SE(3)$, see [27]) is the reference trajectory of the lead robot, $\boldsymbol{r}$ is a set of shape vectors describing the relative positions of each vehicle with respect to the reference formation frame $\{M\}$, and H is a control graph where nodes represent robots and edges represent relations between nodes (see details below and in [17]). Without loss of generality, the formation reference frame $\{M\}$ is fixed to the lead robot; however, it is not a requirement in our method. Sometimes it is necessary to add virtual robots to the group to represent either moving targets, or trajectories that are along such features as walls, lanes, or obstacles.

The control graphs describing the formation are designed from the basic controllers described in the previous section. In Fig. 7, for example, the formation of a group of four robots involves one leader following controller (R_2 following R_1) and two formation shape controllers (R_3 following R_1 and R_2, and R_4 following R_2 and R_3). We call such a directed graph H, with n nodes representing n robots and edges describing the control policy between the connected robots, a control graph. Fig. 7 shows a directed graph represented by its adjacency matrix $\boldsymbol{H}$ (see [19] for definition). Note the control flow from leader i to follower j. If a column j has a nonzero entry in row i, then robot j is following i. A robot can have up to two leaders. Note that $\boldsymbol{H}$ can be written as an upper triangular matrix for any directed acyclic graph (with possible reordering of vertices).

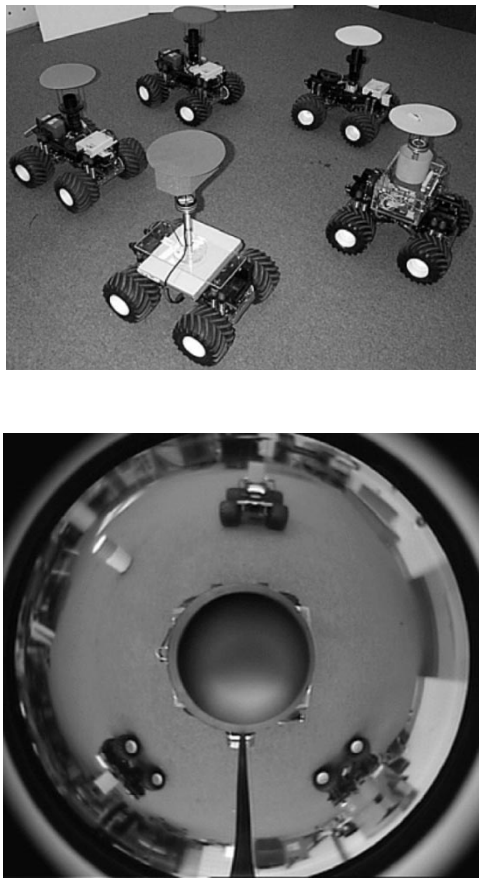

Fig. 11. (top) Clodbuster team used for experiments. (bottom) Typical view from the omnidirectional camera.

For a formation of n robots, we can consider a triangulation approach and Fig. 5 can be used to assign control graphs for labeled robots. For robot R_3, we use Fig. 5. For $k > 3$, we select the two nearest neighbors $\{i, j\}$ from the set $\{1, 2, \ldots, i-1\}$, and select controllers based on l_{ij} and l_{ik}. Fig. 8 shows two example simulations of teams of six robots converging to the desired shape while following the desired trajectory. The robots apply the above technique to reassign the control graph at every timestep while relying on the cooperative localization to reparameterize the shape setpoints for the controllers. The final assignment H is different in the two cases even though the same desired formation shape is achieved.

An obvious concern regarding stability of the formation arises when we switch between control graphs and shape vectors to achieve and maintain a desired physical shape. In Section III-A,

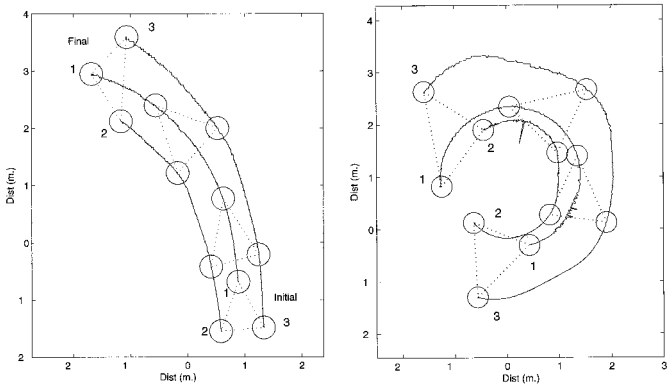

Fig. 12. Sample ground-truth data for trajectories for a triangular formation.

it was shown that under some assumptions on the sensor and motion constraints, the system had a common quadratic Lyapunov function [26] and a stable equilibrium point. While a proof similar to the one for three robots can be pursued for the n robot assignment problem, finding a common Lyapunov function and working through the calculations becomes tedious and does not provide insight into the problem.

IV. Sensing and Estimation

The sole physical sensor used by the robots in our experiments is the onboard catadioptric camera system [28]. From the omnidirectional imagery acquired by these cameras, we have developed several logical sensors—an obstacle detector, a collision detector, a decentralized state observer, and a centralized state observer (see [29]). One of the primary advantages of catadioptric camera systems for this application is that they afford a single effective point of projection. This means that after an appropriate calibration, every point in the omnidirectional image can be associated with a unique ray through the focal point of the camera. As a result, each robot can compute reliable estimates of the direction vectors to its teammates. These directions provide the basis for both centralized and decentralized state observation.

A. Decentralized State Observation

The controllers described in Section II require reliable estimates of the leader robot's (R_i's) linear velocity v_i and angular velocity ω_i by the follower robot R_j and their relative orientation ($\theta_i - \theta_j$). Our algorithm estimates these quantities using an extended Kalman filter [30] based on the range ρ_{ij} and the bearing β_{ij} of the observed leader R_i measured using the omnidirectional camera. The velocity of the observed vehicle is treated as part of the state. In addition, the filter requires a sensor model and the relative kinematics [see (1)] of the leader R_i and follower R_j.

The image processing algorithms provide two observations

$$\begin{aligned}\rho_{ij} &= \sqrt[2]{(x_i - x_j)^2 + (y_i - y_j)^2} \\ \beta_{ij} &= \frac{\pi}{2} + a\tan 2(y_i - y_j, x_i - x_j) - \theta_j. \end{aligned} \tag{16}$$

Next, we differentiate (16) to obtain $\dot{\rho}_{ij}$ and $\dot{\beta}_{ij}$. Using the kinematic (1), our extended state vector then becomes

$$\dot{\bar{\boldsymbol{x}}} = f(\bar{\boldsymbol{x}}, \boldsymbol{u}, \boldsymbol{w}) \tag{17}$$

$$\begin{pmatrix} \dot{\theta}_i \\ \dot{v}_i \\ \dot{\omega}_i \\ \dot{\rho}_{ij} \\ \dot{\beta}_{ij} \\ \dot{\theta}_j \end{pmatrix} = \begin{pmatrix} \omega_i \\ 0 \\ 0 \\ v_i \sin\alpha_{ij} - v_j \sin\beta_{ij} \\ \frac{v_i \cos\alpha_{ij} - v_j \cos\beta_{ij}}{\rho_{ij}} - \omega_j \\ \omega_j \end{pmatrix} + \boldsymbol{w}(t) \tag{18}$$

where $\alpha_{ij} = \beta_{ij} + \theta_j - \theta_i$, $\boldsymbol{w}(t)$ is the process noise, $\boldsymbol{u} = [v_j \quad \omega_j]^T$ is the input vector, and we assume $\dot{v}_i \approx 0$, $\dot{w}_i \approx 0$. The system output with sensor noise is given by

$$\boldsymbol{z}(t) = \boldsymbol{h}(\bar{\boldsymbol{x}}) + \boldsymbol{\eta}(t) = [\rho_{ij} \quad \beta_{ij}]^T. \tag{19}$$

The discrete system becomes

$$\bar{\boldsymbol{x}}(k+1) = \boldsymbol{F}(\bar{\boldsymbol{x}}(k), \boldsymbol{u}(k)) + \boldsymbol{w}(k), \quad \boldsymbol{w}(k) \sim N(0, \boldsymbol{Q}(k)) \tag{20}$$

where $\boldsymbol{F}(\bar{\boldsymbol{x}}(k), \boldsymbol{u}(k))$ is the nonlinear state transition function. $\boldsymbol{w}(k)$ is a noise source assumed to be zero-mean Gaussian with covariance $\boldsymbol{Q}(k)$. We use a sampling interval of $\Delta T \sim 50$ ms. The discrete (observation) output is given by

$$\boldsymbol{Z}(k) = \boldsymbol{h}(\bar{\boldsymbol{x}}(k)) + \boldsymbol{\eta}(k), \quad \boldsymbol{\eta}(k) \sim N(0, \boldsymbol{R}(k)). \tag{21}$$

The covariance $\boldsymbol{R}(k)$ is experimentally determined. We use a standard extended Kalman filter-based estimation algorithm (see, e.g., [31]) to estimate $\hat{\bar{\boldsymbol{x}}}(k+1|k+1)$ and its covariance $\boldsymbol{P}(k+1|k+1)$, given $\hat{\bar{\boldsymbol{x}}}(k|k)$ and $\boldsymbol{P}(k|k)$ at time k and the current observation $\boldsymbol{Z}(k+1)$.

The decentralized state observer provides the follower with necessary information about the velocity of the leader for feedforward control, in addition to the relative position and orientation. This eliminates the need for explicit communication.

B. Centralized State Observation

Approaches to the multirobot localization problem involve estimating pose with respect to each other, the environment, or some combination thereof [1], [32], [33]. Our centralized observer adopts the former approach, relying upon information sharing between robots to solve for the team pose (position and orientation) in closed form. The resulting estimate is more robust than that obtained in the decentralized case, since the state is fully observable with each observation; the need to estimate the velocity for state prediction is eliminated. However, this comes at the cost of communication. In our implementation, the centralized observer uses two methods for estimating the team pose: triangulation-based and pair-wise localization.

Using the triangulation-based method, a team of three (or more) robots is capable of localizing in three-dimensional (3-D) space when each can measure the direction vectors to the other team members. In Fig. 9, the unit vectors $\hat{u}_{ij} \in \mathbb{R}^3$ denote the direction between robot i and robot j expressed in the coordinate frame of robot i. Let ${}^iT_j \in \mathbb{R}^3$ and ${}^iR_j \in SO(3)$ represent, respectively, the translation and rotation of robot j with respect to the frame of reference of robot i. These direction vectors are derived from the images using the procedure described above. Without loss of generality, we can choose the reference frame of robot 1 as our base frame and recover the positions and orientations of the other robots with respect to this frame.

In each frame, the internal angle ψ_i (see Fig. 9) can be determined by a scalar product, e.g., $\psi_2 = \cos^{-1}(\hat{u}_{21} \cdot \hat{u}_{23})$. With this angle information, the translation between the frames can readily be determined up to a scale factor by applying the sine

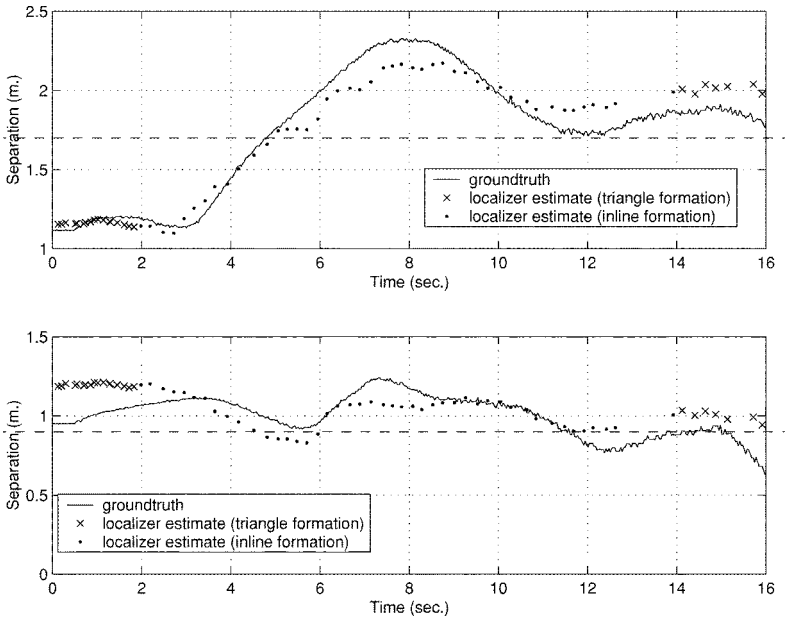

Fig. 13. Follower separation distances: ground-truth versus centralized observer estimates for followers R_2 (top) and R_3 (bottom).

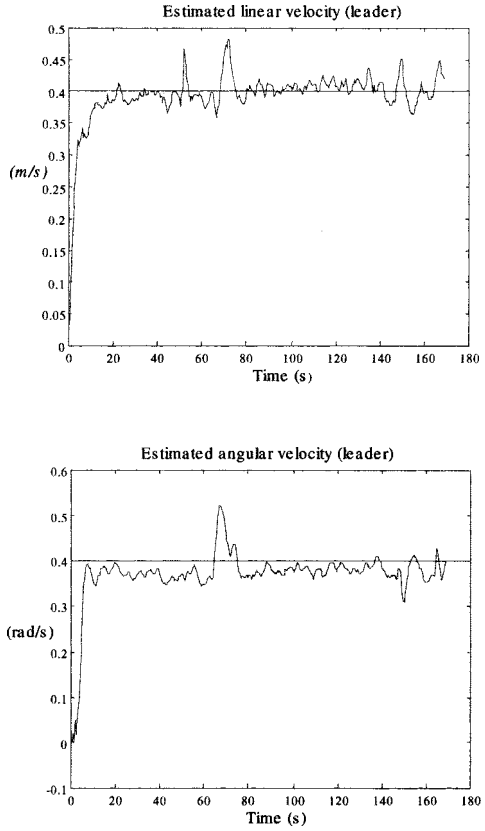

Fig. 14. Leader velocity estimation by the follower. Results are consistent with the actual linear and angular velocities for the leader doing a constant circle (0.4 m/s and circle radius 1.05 m).

rule to the shaded triangle in Fig. 9. Position vectors relative to other frames can also be obtained to within a scale factor by using the corresponding unit vectors.

We thus only require the relative orientations of the frames and the scale factor to complete the localization procedure. To determine the relative orientation of the frames, we note that the vectors ${}^jT_i$ and ${}^iT_j$ should have equal magnitude, but opposite direction when transformed to the same frame. We note a similar relationship between the vectors $({}^jT_i - {}^jT_k)$ and ${}^iT_k$. From these, we obtain the following pairs of equations:

$$\begin{aligned} -{}^1T_2 &= {}^1\boldsymbol{R}_2\,{}^2T_1, \qquad {}^1T_3 - {}^1T_2 = {}^1\boldsymbol{R}_2\,{}^2T_3 \\ -{}^1T_3 &= {}^1\boldsymbol{R}_3\,{}^3T_1, \qquad {}^1T_2 - {}^1T_3 = {}^1\boldsymbol{R}_3\,{}^3T_2. \end{aligned} \tag{22}$$

With all translation vectors known to a scale factor, the problem of solving for each rotation matrix reduces to the form

$$\boldsymbol{R}a_i = b_i \qquad i \in [1,2]. \tag{23}$$

This can be rephrased as the following optimization problem:

$$\min_{R \in SO(3)} \sum_i \left\| \boldsymbol{R}a_i - b_i \right\|^2. \tag{24}$$

The rotation matrix which minimizes this expression can be computed in closed form as follows [34]

$$\boldsymbol{R} = \left(M^T M\right)^{-1/2} M^T \tag{25}$$

where $M = \sum_i a_i b_i^T$.

Again, recall that this solution has so far only required relative bearing information, but yields the pose of the team only to a scale factor. However, in our experiments the robots were constrained to operations in $SE(2)$. We exploit this and the known robot geometry so that any robot could gauge the distance to its teammates based on the radial image distance. As a result, we have a means by which each robot can provide two estimates of the scale (one for each of its visible partners). We use the redundant estimates from all three to obtain the overall scale factor and the relative pose of the team.

This solution offers an improvement over methods presented previously, in that we obtain the relative orientation of the robot team solely from angular measurements, and eliminate the need for additional sensors required to measure orientation in previous implementations [32]. However, it does not eliminate the singularity associated with linear formations. Additionally, it requires that all three robots maintain line of sight. This is a stringent requirement that does not hold in an obstacle-clut-

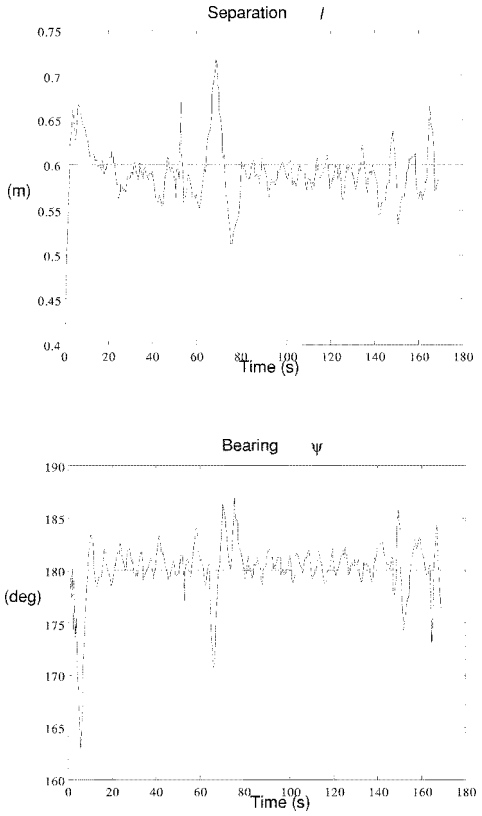

Fig. 15. Follower separation and relative bearing for a feedforward controller. Notice the jump at $t \sim 65$ s as we manually restrained the follower for 5 s. The controller recovers within a few seconds.

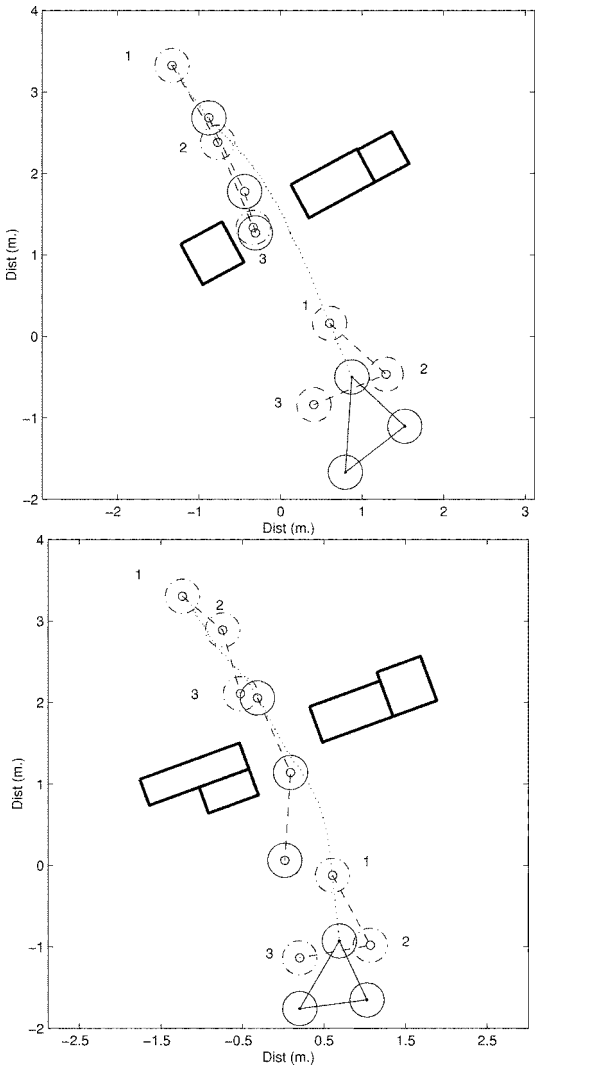

Fig. 16. Ground plane data for formation switching, two runs. The line change from solid to dotted corresponds to the initiation of the switch.

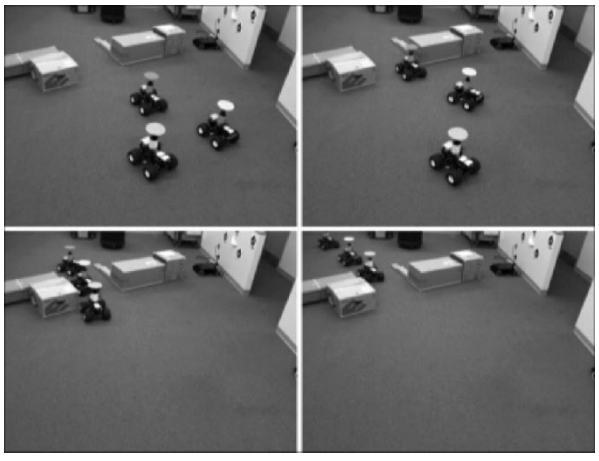

Fig. 17. Triangular to inline formation switch to avoid obstacles.

tered environment. However, we note though that when the pose problem is reduced to 2-D space, relative localization can be accomplished by a pair of robots. Using this fact, our implementation dynamically switches between triangulation-based and pair-wise localization estimation, based on team geometry and the external environment.

Consider the case of a triangular formation approaching a narrow passage through obstacles shown in Fig. 10. A formation switch is ordered to allow the team to proceed through the passage [Fig. 10(a)]. As the robots approach a linear formation, there comes a point where the improved accuracy afforded by exploiting the triangle constraint is compromised by operating in proximity to its singularity. At this point, the centralized observer automatically switches to pair-wise localization mode [Fig. 10(b)]. Robot R_2 exchanges information with the team leader (R_1) to localize relative to the leader's frame. R_3 performs a similar exchange with R_2 and, as a result, determines its pose relative to R_1. While this mode switch resulted from the formation geometry, it can also be directly triggered by the environment. This is shown in Fig. 10(c), where the line of sight between two robots is occluded by an obstacle. This occlusion can be detected from a global visibility matrix, resulting in a pair-wise localization switch.

The pair-wise method serves as the secondary localization mode for the centralized observer. In most formation geometries, the constraint obtained by determining the relative formation scale—along with the redundant range measurements for estimating the absolute scale—result in improved performance in the triangulation-based mode. Mean range errors were typically 3%–5%, compared with 10% for the pair-wise case.

The advantages resulting from this internal switching are twofold. It allows the centralized observer to robustly estimate

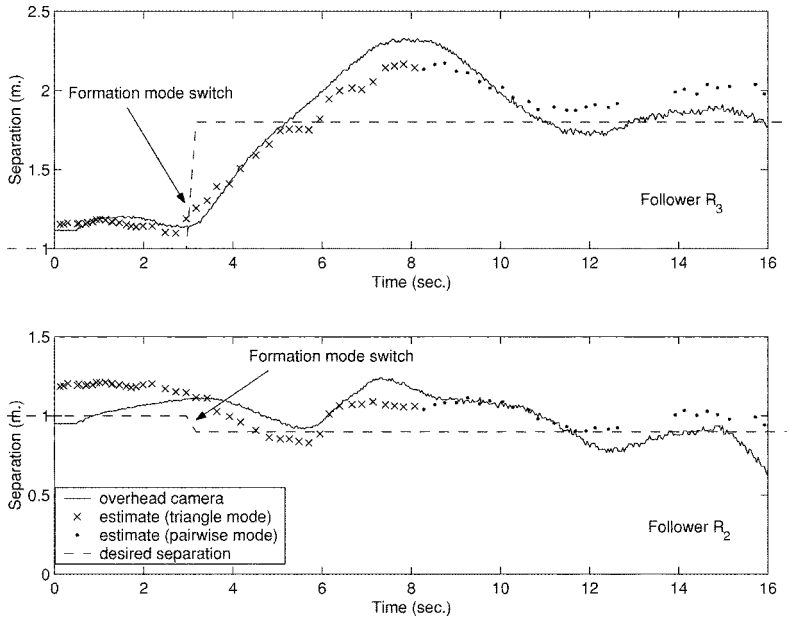

Fig. 18. Ground truth versus centralized observer estimates corresponding to the experiment in Fig. 16.

the team state regardless of formation geometry. Additionally, it allows the team to react to an obstacle-cluttered environment with only a slight degradation in accuracy.

V. Experiments

A. Hardware Platform

The cooperative control framework was implemented on the GRASP Lab's Clodbuster (CB) robots (see Fig. 11). The CB platform is based on the Tamiya CB radio-controlled scale model truck. Video signals from the omnidirectional camera camera are sent to a remote computer via a wireless 2.4–GHz video transmitter. Velocity and heading control signals are sent from the host computer to the vehicles as necessary. This reduces the cost and size of the platform.

Fig. 19. Distributed manipulation demonstration.

B. Formation Control

Initial experiments in formation control were used to validate the dynamic state estimator and corresponding control approach. As a result, we first examined stable formations following trajectories of straight lines and circular arcs. Video data from these trials were recorded using a calibrated overhead camera to provide ground-truth position data of the formation. Data from two trials are shown in Fig. 12.

We next compared the state observer estimates with the ground-truth position data. As an example, in the trial on the left side of Fig. 12, the desired formation was an isosceles triangle where both followers maintained a distance of 1.0 m from the leader. Fig. 13 contrasts the measured leader-follower separation distances with those calculated by the centralized state observer. Results are for the most part satisfactory, with mean separation errors of 3.2% and 5.5% for the two followers. Discontinuities in state observer estimates are due to corrupted image data resulting from the remote video transmission. Typical image corruption rates were 15%–20% for each robot, leaving periods of time where no localization was possible. Also worth noting is that the actual separation distance of the robots is always greater than desired. This is due to the pure feedback controller used with the centralized observer.

Additional experiments with the decentralized observer, which includes velocity estimates, were also conducted. Shown in Figs. 14 and 15, the lead robot executes a circle while the follower attempts to maintain 0.6-m separation and a relative bearing of 180°. The controller response is significantly improved as a result of the feedforward terms from the estimator. We also examined the robustness of the estimator by manually restraining the follower at $t \sim 65$ s. As can be seen from the plots, the system recovered quickly.

These results suggest that both observers provide sufficiently good state estimates. However, despite the superior estimator performance, the control response for the centralized case is compromised by the lack of a feedforward component. We are currently integrating a velocity estimator to address this.

C. Switching Formations

In these experiments, the lead robot is to perform an exploratory mission while the formation shape changes in a decentralized fashion as required by the environment. We use a simple reactive obstacle avoider [24] on the leader, while allowing the team to choose between either an isosceles triangle or inline convoy formation. In the presence of obstacles, the followers switch to an inline position behind the leader in order to negotiate the obstacles while following the leader. See Figs. 16 and 17. The internal mode switching in our centralized state observer is also shown in Fig. 18. Approximately 3 s into the run, the leader detects the obstacles and triggers a formation switch (triangle to inline). The observer mode switches internally from triangular to pair-wise depending on the geometry of the formation.

D. Coordinated Manipulation

The ability to maintain a prescribed formation allows the robots to "trap" objects in their midst and to flow the formation, guaranteeing that the object is transported to the desired position. With this in mind, we proceeded to apply this technique to a manipulation application. Experiments were conducted using a box as the object to be manipulated. In Fig. 19, the initial team configuration is centered around the box, with the goal to flow the now-encumbered formation along a trajectory generated by the leader. By choosing a constraining formation geometry, the box is kept in contact with all three robots during the formation flow. Several snapshots from a sample run are shown in Fig. 19. Despite the control strategy not accounting for changes in the object pose, the formation was typically successful in its manipulation task over the tested trajectories. These experiments, while not an exhaustive investigation of distributed manipulation, demonstrate the potential for a vision-based formation control application.

VI. Conclusion

In this paper, we propose a framework for the development of intelligent multirobot systems by composing simple sensing, estimation, control, and coordination blocks in a bottom-up approach. The main contributions are a suite of control and estimation algorithms, and a paradigm for switching that allows a group of robots to maintain a prescribed formation (shape and size) while following a planned trajectory. The switching paradigm also allows the robots to change formation in the presence of obstacles. A distinguishing feature of our work is the fact that each robot relies only on a single omnidirectional camera for sensory information. We have demonstrated our framework in cooperative tasks like exploration and manipulation. Because our controllers and estimators can be decentralized and the framework allows the selection of the best controller and estimator in a given situation, our framework can potentially scale to groups of tens and hundreds of robots. Analyzing the effect of communication constraints, deciding the optimality of formation choices for a given environment, sensor planning for cooperative active vision, and implementing multirobot coordination tasks with a larger number of robots are also important directions for our future work.

Acknowledgment

The authors would like to thank B. Southall, J. Esposito, G. Grudic, K. McIsaac, P. Song, and Z. Wang for discussions on multirobot cooperation and control.

References

[1] D. Fox, W. Burgard, H. Kruppa, and S. Thrun, "A probabilistic approach to collaborative multi-robot localization," *Auton. Robots*, vol. 8, no. 3, pp. 325–344, June 2000.

[2] J. Feddema and D. Schoenwald, "Decentralized control of cooperative robotic vehicles," presented at the SPIE, vol. 4364, Aerosense, Orlando, FL, Apr. 2001.

[3] J. S. Jennings, G. Whelan, and W. F. Evans, "Cooperative search and rescue with a team of mobile robots," in *Proc. IEEE Int. Conf. Advanced Robotics*, 1997, pp. 193–200.

[4] D. Rus, B. Donald, and J. Jennings, "Moving furniture with teams of autonomous robots," in *Proc. IEEE/RSJ Int. Conf. Intelligent Robots and Systems*, Pittsburgh, PA, Aug. 1995, pp. 235–242.

[5] M. Mataric, M. Nilsson, and K. Simsarian, "Cooperative multi-robot box pushing," in *Proc. IEEE/RSJ Int. Conf. Intelligent Robots and Systems*, Pittsburgh, PA, Aug. 1995, pp. 556–561.

[6] D. Stilwell and J. Bay, "Toward the development of a material transport system using swarms of ant-like robots," in *Proc. IEEE Int. Conf. Robotics and Automation*, Atlanta, GA, May 1993, pp. 766–771.

[7] T. Sugar and V. Kumar, "Control and coordination of multiple mobile robots in manipulation and material handling tasks," in *Experimental Robotics VI: Lecture Notes in Control and Information Sciences*, P. Corke and J. Trevelyan, Eds. New York: Springer-Verlag, 2000, vol. 250, pp. 15–24.

[8] A. De Luca, G. Oriolo, and C. Samson, "Feedback control of a nonholonomic car-like robot," in *Robot Motion Planning and Control*, J.-P. Laumond, Ed. London: Springer-Verlag, 1998, pp. 171–253.

[9] R. Murray, Z. Li, and S. Sastry, *A Mathematical Introduction to Robotic Manipulation*. Boca Raton, FL: CRC, 1994.

[10] J.-J. E. Slotine and W. Li, *Applied Nonlinear Control*. Englewood Cliffs, NJ: Prentice-Hall, 1991.

[11] R. Brooks, "A robust layered control system for a mobile robot," *IEEE J. Robot. Automat.*, vol. RA–2, pp. 14–23, Feb. 1986.

[12] T. Balch and R. Arkin, "Behavior-based formation control for multirobotic teams," *IEEE Trans. Robot. Automat.*, vol. 14, pp. 926–934, Dec. 1998.

[13] L. E. Parker, "Current state of the art in distributed autonomous mobile robotics," in *Distributed Autonomous Robotic Systems*, L. E. Parker, G. Bekey, and J. Barhen, Eds. Tokyo, Japan: Springer-Verlag, 2000, vol. 4, pp. 3–12.

[14] P. Tabuada, G. Pappas, and P. Lima, "Feasible formations of multi-agent systems," in *Proc. American Control Conf.*, Arlington, VA, June 2001, pp. 56–61.

[15] T. Balch, "Social potentials for scalable multi-robot formations," in *Proc. IEEE Int. Conf. Robot. Automat.*, Apr. 2000, pp. 73–80.

[16] H. Yamaguchi and T. Arai, "Distributed and autonomous control method for generating shape of multiple mobile robot group," in *Proc. IEEE Int. Conf. Intelligent Robots and Systems*, vol. 2, 1994, pp. 800–807.

[17] J. P. Desai, J. P. Ostrowski, and V. Kumar, "Modeling and control of formations of nonholonomic mobile robots," *IEEE Trans. Robot. Automat.*, vol. 17, pp. 905–908, Dec. 2001.

[18] F. E. Schneider, D. Wildermuth, and H.-L. Wolf, "Motion coordination in formations of multiple mobile robots using a potential field approach," in *Distributed Autonomous Robotic Systems*, L. E. Parker, G. Bekey, and J. Barhen, Eds. Tokyo, Japan: Springer-Verlag, 2000, vol. 4, pp. 305–314.

[19] J. Desai, V. Kumar, and J. P. Ostrowski, "Control of changes in formation for a team of mobile robots," in *Proc. IEEE Int. Conf. Robotics and Automation*, Detroit, MI, May 1999, pp. 1556–1561.

[20] R. Fierro, P. Song, A. K. Das, and V. Kumar, "Cooperative control of robot formations," in *Cooperative Control and Optimization*, R. Murphey and P. Pardalos, Eds. Dordrecht, The Netherlands: Kluwer, 2002, ch. 5, pp. 73–93.

[21] R. Burridge, A. Rizzi, and D. Koditschek, "Sequential composition of dynamically dexterous robot behaviors," *Int. J. Robot. Res.*, vol. 18, no. 6, pp. 534–555, June 1999.

[22] K. H. Tan and M. A. Lewis, "Virtual structures for high precision cooperative mobile robot control," *Auton. Robots*, vol. 4, pp. 387–403, Oct. 1997.

[23] J. Lawton, B. Young, and R. Beard, "A decentralized approach to elementary formation manuevers," in *Proc. IEEE Int. Conf. Robotics and Automation*, San Francisco, CA, Apr. 2000, pp. 2728–2733.
[24] A. Das, R. Fierro, V. Kumar, J. Southall, J. Spletzer, and C. J. Taylor, "Real-time vision based control of a nonholonomic mobile robot," in *Proc. IEEE Int. Conf. Robotics and Automation*, May 2001, pp. 1714–1719.
[25] W. E. Dixon, D. M. Dawson, and E. Zergeroglu, "Robust control of a mobile robot system with kinematic disturbances," in *IEEE Int. Conf. Control Applications*, Anchorage, AK, Sept. 2000, pp. 437–442.
[26] D. Liberzon and A. S. Morse, "Basic problems in stability and design of switched systems," *IEEE Contr. Syst.*, vol. 19, pp. 59–70, Oct. 1999.
[27] R. Fierro, C. Belta, J. Desai, and V. Kumar, "On controlling aircraft formations," in *Proc. IEEE Conf. Decision and Control*, Orlando, FL, Dec. 2001, pp. 1065–1070.
[28] S. Baker and S. Nayar, "A theory of catadoptric image formation," in *Proc. Int. Conf. Computer Vision*, Bombay, India, Jan. 1998, pp. 35–42.
[29] R. Alur, A. Das, J. Esposito, R. Fierro, Y. Hur, G. Grudic, V. Kumar, I. Lee, J. P. Ostrowski, G. Pappas, J. Southall, J. Spletzer, and C. J. Taylor, "A framework and architecture for multirobot coordination," in *Experimental Robotics VII*, D. Rus and S. Singh, Eds. New York: Springer-Verlag, 2001, pp. 303–312.
[30] G. M. Souris, *An Engineering Approach to Optimal Control and Estimation Theory*. New York: Wiley, 1996.
[31] J. J. Leonard and H. F. Durrant-Whyte, *Directed Sonar Sensing for Mobile Robot Navigation*. Boston, MA: Kluwer, 1992.
[32] R. Kurazume and S. Hirose, "Study on cooperative positioning system—Optimum moving strategies for CPS III," in *Proc. IEEE Int. Conf. Robotics and Automation*, Leuven, Belgium, May 1998, pp. 2896–2903.
[33] S. I. Roumeliotis and G. A. Bekey, "Distributed multi-robot localization," in *Distributed Autonomous Robotic Systems*, L. E. Parker, G. Bekey, and J. Barhen, Eds. Tokyo, Japan: Springer-Verlag, 2000, vol. 4, pp. 179–188.
[34] A. Nadas, "Least Squares and Maximum Likelihood Estimation of Rigid Motion," IBM Tech. Rep., 1978.

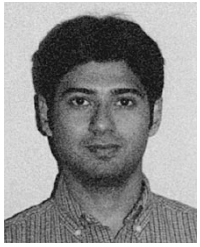

Aveek K. Das (S'01) received the B.E. degree in mechanical engineering from Birla Institute of Technology and Sciences, Pilani, India, in 1997, and the M.S. degree in mechanical engineering and applied mechanics from the University of Pennsylvania, Philadelphia, in 1999. He is currently a Ph.D. degree candidate at the University of Pennsylvania.

His research interests include vision-based control, hybrid formation control, and ad hoc communication networks for mobile robots.

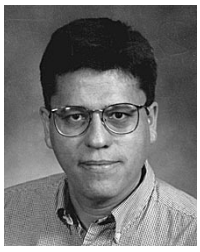

Rafael Fierro (S'95–M'97) received the Ph.D. degree in electrical engineering from the University of Texas, Arlington, in 1997.

Between December 1999 and July 2001, he held a Postdoctoral Research appointment with the GRASP Lab, University of Pennsylvania, Philadelphia. He is currently an Assistant Professor in the School of Electrical and Computer Engineering at Oklahoma State University, Stillwater. His research interests include hybrid and embedded systems, robotics, and distributed control of autonomous vehicles.

Dr. Fierro is the recipient of a British Council Scholarship and Fulbright Scholarship.

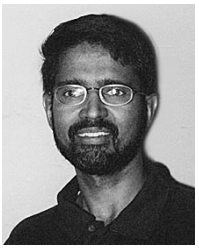

Vijay Kumar (S'87–M'87–SM'02) received the M.S. and Ph.D. degrees in mechanical engineering from Ohio State University, Columbus, in 1985 and 1987, respectively.

He is currently a Professor in the Department of Mechanical Engineering and Applied Mechanics with a secondary appointment in the Department of Computer and Information Science at the University of Pennsylvania, Philadelphia.

Dr. Kumar has served on the editorial board of the IEEE TRANSACTIONS ON ROBOTICS AND AUTOMATION, the editorial board of the J*ournal of the Franklin Institute*, and the ASME *Journal of Mechanical Design*. He is the recipient of the 1991 National Science Foundation Presidential Young Investigator award and the 1997 Freudenstein Award for significant accomplishments in mechanisms and robotics.

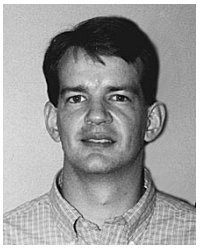

James P. Ostrowski (S'90–M'90) received the Sc.B. degree from Brown University, Providence, RI, in 1986 and the M.S. and Ph.D. degrees from the California Institute of Technology, Pasadena, in 1991 and 1996, respectively.

He is an Associate Professor in the Department of Mechanical Engineering and Applied Mechanics at the University of Pennsylvania, Philadelphia, and holds a secondary appointment in the Department of Computer and Information Science. His expertise is in the areas of nonlinear dynamics and control for robotics, with a particular emphasis on the mechanics and control of robotic locomotion systems and sensor-based control and planning for multirobot systems and blimps.

Dr. Ostrowski is currently an Associate Editor for the IEEE TRANSACTIONS ON ROBOTICS AND AUTOMATION, and is the recipient of an NSF CAREER award.

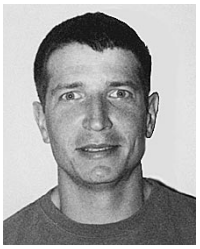

John Spletzer received the B.S. degree in mechanical engineering from Temple University, Philadelphia, PA, in 1989. He received the M.S. degree in mechanical engineering from the Johns Hopkins University, Baltimore, MD, in 1993. In 1999, he received the M.S. degree in computer and information science from the University of Pennsylvania, Philadelphia.

In 1993, he was a Test Engineer for the U.S. Army Test and Evaluation Command. He is currently a Ph.D. degree candidate at the University of Pennsylvania. His research interests include autonomous robots and sensor planning.

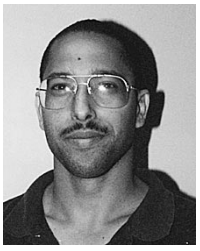

Camillo J. Taylor (S'89–M'92) received the A.B. degree in electrical, computer and systems engineering from Harvard University, Cambridge, MA, in 1988, and the M.S. and Ph.D. degrees from Yale University, New Haven, CT, in 1990 and 1994, respectively.

He is currently an Assistant Professor in the Computer Information Science Department at the University of Pennsylvania. From 1994 to 1997, he was a Postdoctoral Researcher and Lecturer with the Department of Electrical Engineering and Computer Science at the University of California, Berkeley. His research interests include reconstruction of 3–D models from images, autonomous vision-guided motor vehicles, and multirobot coordination.